NANO LETTERS

pubs.acs.org/NanoLett

Letter

Acoustothermal Nucleation of Surface Nanobubbles

Saikat Datta,* Rohit Pillai,* Matthew K. Borg,* and Khellil Sefiane*

Cite This: *Nano Lett.* 2021, 21, 1267−1273

Read Online

ACCESS | Metrics & More | Article Recommendations | Supporting Information

ABSTRACT: Ultrasonic surface vibration at high frequencies (O(100 GHz)) can nucleate bubbles in a liquid within a few nanometres from a surface, but the underlying mechanism and the role of surface wettability remain poorly understood. Here, we employ molecular simulations to study and characterize this phenomenon, which we call acoustothermal nucleation. We observe that nanobubbles can nucleate on both hydrophilic and hydrophobic surfaces, and molecular energy balances are used to identify whether these are boiling or cavitation events. We rationalize the nucleation events by defining a physics-based energy balance, which matches our simulation results. To characterize the interplay between the acoustic parameters, surface wettability, and nucleation mechanism, we produce a regime map of nanoscopic nucleation events that connects observed nanoscale results to macroscopic experiments. This work provides insights to better design a range of industrial processes and clinical procedures such as surface treatments, mass spectroscopy, and selective cell destruction.

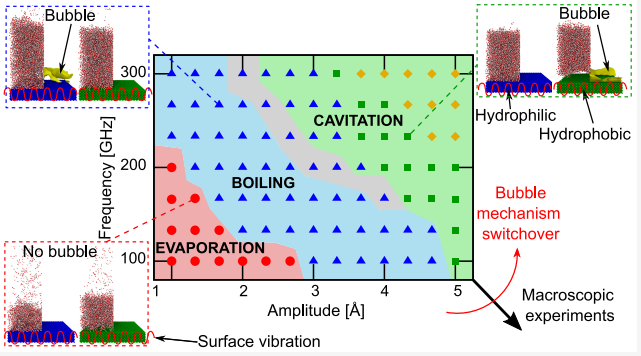

KEYWORDS: *acoustothermal nucleation, boiling, cavitation, nanobubbles, vibrations, wettability*

Ultrasonic vibration of a wetted surface results in rapid pressure fluctuations inside the liquid and can nucleate bubbles in local regions that drop below the vapor pressure.[1−7] These bubbles are unstable and generate powerful shock waves as they collapse, which has applications in industrial and chemical processes, such as nanocomposite synthesis,[8] enhancement of chemical reactions,[9] dental plaque cleaning,[10] and drug delivery.[11] We recently discovered that extremely high frequency vibrations can also nucleate bubbles at the nanoscale by heating,[12] i.e., when the temperature in local regions exceeds the liquid's boiling point. This heating occurs because surface vibrations dissipate energy into the liquid via viscous dissipation locally near the surface, which gains importance when the liquid film dimensions drop below the Stokes boundary layer height, $h_{st} = \sqrt{\mu/\rho\omega}$,[13] where ρ is the liquid density, μ is the dynamic viscosity, and ω is the angular vibrational frequency (see Figure 1A).[12,14−17] High acoustothermal heat fluxes can be generated for small amounts of liquid vibrated at high frequencies (up to ~10^9 W/m^2 for water nanofilms vibrated at O(100 GHz)[12]), which can rapidly take the liquid to the vicinity of the liquid−vapor spinodal, causing explosive bubble nucleation or boiling. This phenomenon of vibration-driven boiling can replace laser-irradiation-driven phase change in a range of applications, such as steam cleaning of surfaces,[18] creating micro/nano-surface patterns,[19] selective killing of biological cells,[20,21] cell perforation,[22−24] distillation,[25] nanowire manipulation,[26] and heterogeneous catalysis.[27] This can also be useful for desorption and ejection of large biomolecules in mass spectroscopy, surgery,

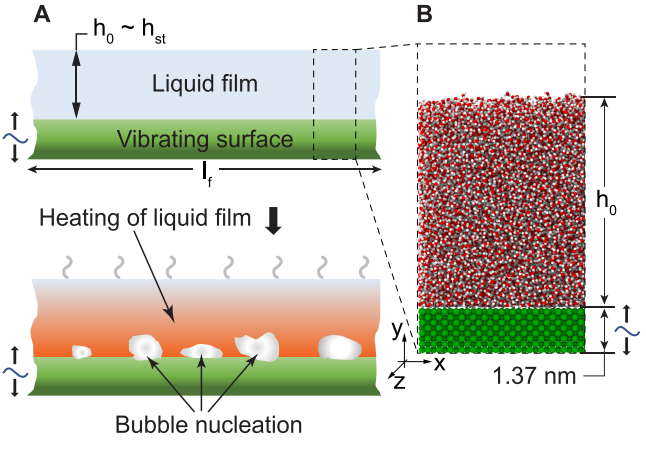

Figure 1. (A) Schematic of the acoustothermal nucleation in a nanofilm and (B) initial configuration of the system considered for the MD simulations. In the simulation domain, a water film of height h_0 = 7 nm is placed on a solid surface of lateral dimensions l_f = 9.4 nm. Further details of the MD simulation setup are provided in the Supporting Information.

Received: September 27, 2020
Revised: December 22, 2020
Published: January 25, 2021

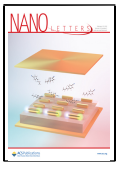

https://dx.doi.org/10.1021/acs.nanolett.0c03895
Nano Lett. 2021, 21, 1267−1273

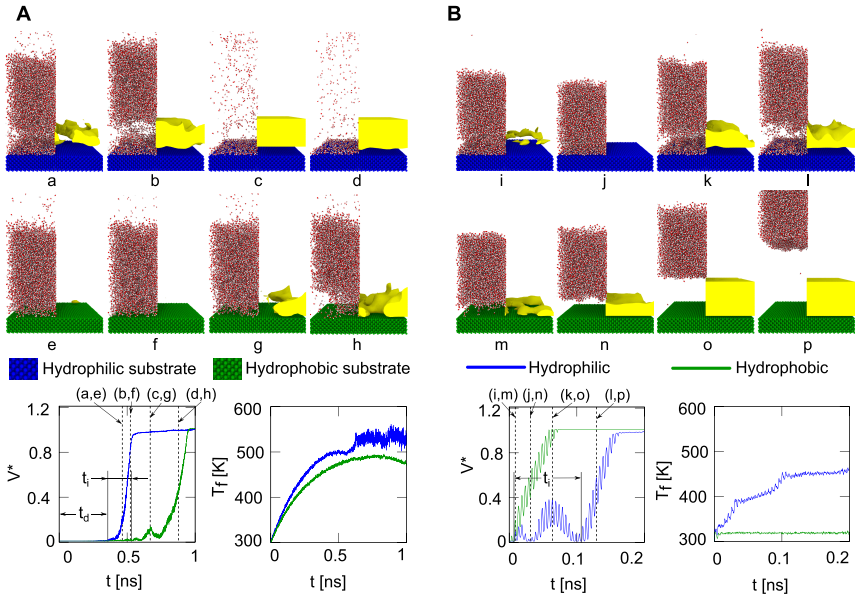

Figure 2. Snapshots of acoustothermal nucleation and film formation in conjunction with line plots showing time variation of normalized bubble volume V^* and film temperature T_f for two representative cases where (A) initiation of steady growing bubbles is observed first on a hydrophilic surface (with $a = 0.1$ nm and $f = 300$ GHz) and (B) initiation of steady growing bubbles is observed first on a hydrophobic surface (with $a = 0.4$ nm and $f = 200$ GHz); in the snapshots, molecules are shown only for half of the domain, while the interface of the nascent bubble is shown on the other half using a yellow iso-density surface. Here, t_d represents the delay period before the onset of a stable bubble nucleation, while t_i is the time interval between the onset of a stable bubble on the hydrophilic and hydrophobic surfaces. Unlike the other cases, for the hydrophobic surface in (B), the detachment of the liquid film (at low T_f) from the surface stops energy flow into it, therefore causing T_f to be constant at the initial temperature of 300 K.

and protein sequencing, where accurate temperature control is necessary during nucleation to avoid unwanted damage of biological tissues.[28] However, for this vision to be realized, a fundamental question needs to be answered: *what are the mechanisms of acoustothermal phase change at high frequencies in thin water films?*

An additional complexity to vibration-based nucleation, be it pressure- or heat-driven, is the role of surface wettability, which has long been recognized as a parameter influencing the onset of nucleation.[29,30] While there is extensive literature on its role in boiling heat transfer,[31−39] there remains an apparent contradiction that is yet to be resolved. Experiments suggest that, when compared to hydrophilic surfaces, the onset of nucleate boiling occurs at a lower temperature[31−36] (and cavitation occurs at a lower vibration threshold[2,3]) for hydrophobic surfaces. This has a clear theoretical justification; the reversible work required to generate a liquid−vapor interface is lower for heterogeneous nucleation on a hydrophobic surface when compared to a hydrophilic one. Therefore, from classical nucleation theory, a lower wall superheat or vibration threshold is required for vapor bubble formation on a hydrophobic surface. However, molecular dynamics studies have demonstrated that the opposite occurs at the nanoscale,[40−42] i.e., that nucleation on hydrophilic surfaces occurs at a lower temperature than on hydrophobic surfaces. The improved momentum transfer from the heated surface, owing to the strong intermolecular interactions, explains these findings. This leads to the second fundamental question that we aim to answer here: *how does wettability mediate bubble formation in the context of acoustothermal heating, i.e., a process which contains both acoustics (vibrations) and heating (viscous dissipation)?*

This Letter aims to shed light on these two fundamental questions, namely, the mechanism of onset of nucleation or bubble formation and the role of surface wettability, using nonequilibrium molecular dynamics (MD) simulations. The MD setup is composed of a nanoscale water film supported by a solid surface, as shown in Figure 1B. Finite-size effects are avoided as detailed in the Supporting Information (SI). Both the liquid and the solid are initiated at $T_0 = 300$ K. No restriction is imposed on the temperature of the system, allowing it to evolve dynamically with the vibrational excitations.

Surface acoustic wave (SAW) devices used in microfluidics applications are typically operated with micrometer-scale wavelengths. The MD setup represents a small spanwise portion of such a device; therefore, the width of the domain is considerably smaller than the wavelengths used. The motion generated by a SAW can therefore be approximated here by a vertical oscillatory motion $y = y_0 + a\sin(2\pi ft)$, with amplitude a and frequency f imparted to the solid surface about its mean equilibrium position y_0. Here, two surfaces with different solid−liquid affinities (hydrophobic and hydrophilic) are used to resolve the interplay between the wettability and the vibrational parameters on bubble nucleation. Most real surfaces contain micro-to-nano-scale cavities, which entrap gas to form nucleation sites. The volume of entrapped gas is inversely proportional to wettability; this is why, in experiments, greater nucleation sites are observed on hydrophobic surfaces than hydrophilic surfaces. In the current study, we choose a perfectly smooth surface to analyze the effect of wettability alone. A systematic study is performed across a wide range of vibrational parameters by tracking the temporal evolution of nascent bubble volume V.

Figure 2 shows snapshots of phase transition along with the time evolution of normalized bubble volume $V^* = V/V_0$ (details on calculating V and the reference volume V_0 are provided in the SI) and the overall film temperature for two representative acoustic cases ($a = 0.1$ nm and $f = 300$ GHz in Figure 2A; $a = 0.4$ nm and $f = 200$ GHz in Figure 2B). Regardless of the acoustic

https://dx.doi.org/10.1021/acs.nanolett.0c03895
Nano Lett. 2021, 21, 1267−1273

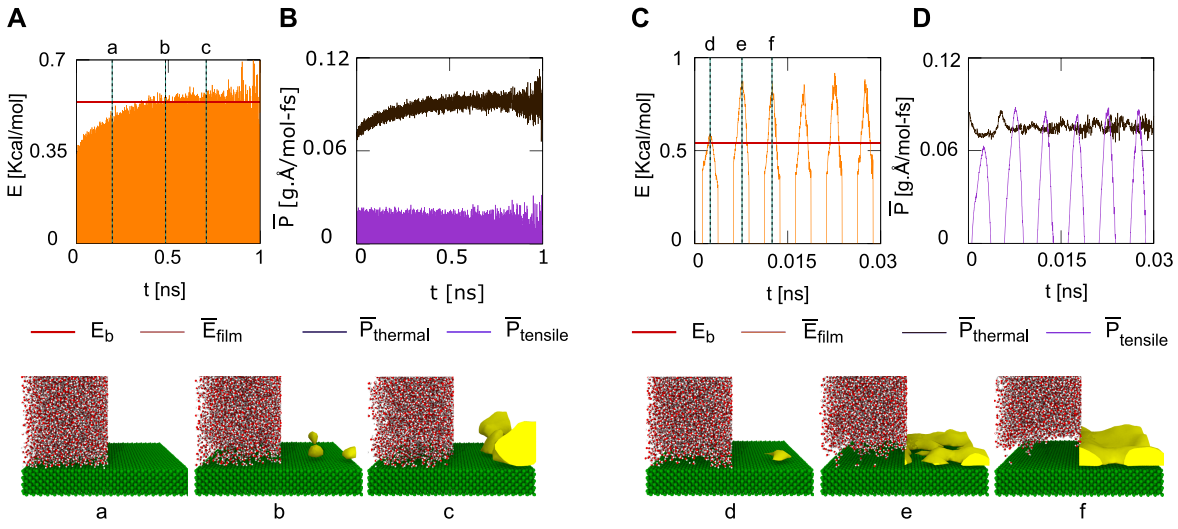

Figure 3. (A) Comparison of energy barrier E_b (red line) and time evolution of mean molecular kinetic energy relative to the moving surface $\bar{E}_{film}$ for acoustothermal nucleation via boiling (orange line). (B) Temporal variation of the momentum due to thermal motion ($\bar{P}_{thermal}$) and mean velocity relative to the surface ($\bar{P}_{tensile}$) for the cases shown in (A). (C) Comparison of energy barrier E_b (red line) and time evolution of mean molecular kinetic energy relative to the moving surface $\bar{E}_{film}$ for acoustothermal nucleation via cavitation (orange line). (D) Temporal variation of the momentum due to thermal motion ($\bar{P}_{thermal}$) and mean velocity relative to the surface ($\bar{P}_{tensile}$) for the cases shown in (C) ((A, B) f = 300 GHz, a = 0.1 nm, hydrophobic surface; (C, D) f = 200 GHz, a = 0.4 nm, hydrophobic surface).

parameters and surface wettability, the nucleation phenomenon starts with one or multiple stable vapor bubbles (i.e., a bubble of nonzero volume that does not collapse completely in the simulation) forming in the vicinity of the surface (Figure 2a on the hydrophilic surface, and Figures 2g and 2m on the hydrophobic surface). The stable bubbles subsequently coalesce and grow until the domain boundary is reached, forming a vapor film between the liquid and surface (Figures 2b, l, h, and n), and the liquid film eventually detaches from the surface (Figures 2c, d, and o). The line plots for the temporal evolution of bubble volume (Figures 2A and 2B) show that stable bubbles form following a delay period t_d after the initiation of vibrational excitation. Each case shows a monotonic volumetric growth after stable bubble formation, reaching a constant volume as the vapor film forms.

Importantly, the nucleation and subsequent growth to a stable vapor bubble is first observed on the hydrophilic surface in Figure 2A but on the hydrophobic surface in Figure 2B. Two important conclusions can be drawn from this. (a) For identical acoustic parameters, it is possible for either hydrophobic or hydrophilic surfaces to have a smaller delay period, t_d, and (b) the preference of nucleation on different wetting surfaces is altered by small changes in acoustic parameters (in contrast to macroscopic vibrational experiments, in which the nucleation always occurs on a hydrophobic surface[2,3]). This switchover of preferred nucleation site can be quantified by the time interval $t_i = (t_d)_{hydrophilic} - (t_d)_{hydrophobic}$, where $t_i \sim 0.2$ ns for Figure 2A and $t_i \sim -0.1$ ns for Figure 2B. Note that the rate at which the liquid molecules gain energy for nucleation determines both t_d and t_i. For high values of a and f, the rate of energy transfer is high, resulting in small values of t_i and t_d; in contrast, low values of a and f, such as those used in macroscale experiments, cause a low rate of energy transfer, thereby producing larger values of t_d and t_i.

The time evolution of the liquid film temperature T_f in Figure 2A shows a significant rise both for hydrophilic ($T_{f,max} \sim 510$ K) and hydrophobic ($T_{f,max} \sim 490$ K) surfaces with $(dT_f/dt)_{hydrophilic} > (dT_f/dt)_{hydrophobic}$; the maximum film temperatures are close to the experimentally observed limit (553−583 K) of metastability in the liquid−vapor phase transition of water at atmospheric pressure.[43] In contrast, $T_{f,max}$ is lower on the hydrophilic surface in Figure 2B compared to that in Figure 2A and negligible on the hydrophobic surface in Figure 2B. These are all indications of predominantly different mechanisms of phase transition, namely, boiling and cavitation, at distinct vibrational conditions. While Figure 2A represents boiling, where the kinetic energy of the molecules play the dominant role, Figure 2B represents cavitation, primarily caused by the tensioned film. This is the reason we observe a switchover in t_i between Figures 2A and 2B.

Measuring local pressure to support our cavitation/boiling switchover hypothesis was not possible, due to the significant thermal noise and the complex continuous motion of the surface. Furthermore, the disjoining pressure in the liquid film due to the van der Waals forces exerted by the solid surface is significant, quantified as

$$P_D = -\frac{\Pi}{6\pi h_d^{\ 3}} \tag{1}$$

where h_d is the height from the solid substrate and Π is the Hamaker constant. The disjoining pressure is dominant over the external pressure in normal operating conditions, which increases the spinodal temperature for phase transition at the vicinity of the solid surface.[44,45] Therefore, the large gradient of disjoining pressure ($P_D \propto 1/h_d^{\ 3}$) across the film thickness next to the surface produces erroneous results for the spatial averaging of pressure over the entire film. Estimation of the local superheating is also not feasible in the current scenario because it requires an accurate calculation of the saturation temperature, which in turn depends on accurate pressure measurements. Therefore, we instead use a dynamic energy balance to obtain the microscopic details of acoustothermal phase transition, which we explain below.

https://dx.doi.org/10.1021/acs.nanolett.0c03895
Nano Lett. 2021, 21, 1267−1273

The key insight into the cavitation/boiling switchover phenomenon we observe is that, at the nanoscale, the molecules of the liquid film closest to a solid surface ordinarily adhere well due to van der Waals interactions. Therefore, the formation of a bubble occurs as a result of liquid molecules "escaping" the attraction of the solid molecules (i.e., work of adhesion), overcoming the energy barrier and nucleating regions of vapor-filled space. To quantify this mechanism, we use the solid−liquid interaction to calculate an energy barrier E_b, which predicts the generation of a stable vapor bubble (see measurement details in SI). As expected, the stronger solid−liquid interaction causes the hydrophilic surface to possess a higher energy barrier compared to a hydrophobic surface. We propose that the energy of the liquid molecules should be $\sim E_b$ to escape from the surface and nucleate a bubble. Nucleation can therefore be studied by tracking the energy or the velocity of the liquid and solid molecules. We define three parameters, namely, $\overline{E}_{film}$, the energy of the film near the surface due to the velocity of the liquid molecules relative to the surface; $\overline{P}_{thermal}$, the momentum due to thermal motion of the liquid molecules; and $\overline{P}_{tensile}$, the momentum of liquid molecules due to their velocity relative to the solid motion, representing the extent of tensile force on the liquid film (see details in SI). Using these measurements along with our energy barrier calculation, we are now able to explain the cavitation/boiling switchover seen in Figure 2. Figures 3A and 3B depict the evolution of $\overline{E}_{film}$, $\overline{P}_{thermal}$, and $\overline{P}_{tensile}$, respectively, for f = 300 GHz and a = 0.1 nm; Figures 3C and 3D track the $\overline{E}_{film}$, $\overline{P}_{thermal}$, and $\overline{P}_{tensile}$ for f = 200 GHz and a = 0.4 nm. As the surface vibrates, the liquid film is subjected to compression and tension during each cycle of oscillation. The compression on the film tries to collapse the bubbles, while the tension on the film favors nucleation. Therefore, we plot $\overline{E}_{film}$ and $\overline{P}_{tensile}$ only during the downward motion of the solid surface to track nucleation events. The variation of $\overline{E}_{film}$ with time appears as a series of spikes, where each spike corresponds to a single oscillation of the surface. Figures 3A and 3C both represent the temporal evolution of $\overline{E}_{film}$ as it approaches E_b, while Figure 3A is more dense as the energy increases gradually and greater number of oscillations are required before E_b is breached. Note that no bubble is observed while $\overline{E}_{film} < E_b$ (Figure 3a), validating our derived energy-barrier calculation. The formation of one or multiple vapor bubbles occurred at $\overline{E}_{film} = E_b$ (Figure 3b), which subsequently grew and coalesced to form a larger bubble with increasing $\overline{E}_{film}$ (Figure 3c). $P_{tensile}$ does not change significantly in Figure 3B; however, the variation of $\overline{P}_{thermal}$ indicates an increasing trend corresponding to the rise of T_f. As the change of $\overline{P}_{thermal}$ is higher than that of $\overline{P}_{tensile}$ in this case (Figure 3B), we characterize the mode of phase transition as boiling, because molecules' thermal motion dominates over the tensioning of the liquid film. Similarly, the time evolution of $\overline{E}_{film}$ in Figure 3C shows a stable vapor phase when $\overline{E}_{film} > E_b$ (Figure 3e, f). However, the variation in $\overline{P}_{tensile}$ is substantial compared to that of $\overline{P}_{thermal}$ in Figure 3D, signifying the predominance of tensioning caused by the surface motion over the thermal motion of the molecules in the phase transition. Therefore, we identify this phase transition to be cavitation. In summary, acoustothermal nucleation occurs due to an increase of molecular kinetic energy in conjunction with liquid tensioning; the relative predominance of either of the two can be controlled by varying the acoustic parameters. Therefore, the temperature during nucleation can be controlled precisely.

To probe the influence of surface wettability on acousto-thermal nucleation, we measure the energy balance of the system by computing the total energy gain ΔE_{total} and work done W_d by the vibrating surface. W_d is the amount of energy transferred to the system and by the second law of thermodynamics should be equal to ΔE_{total} (see SI for more details). Here, ΔE_{total} is given by

$$\Delta E_{total} = \Delta PE_{film} + \Delta KE_{film} + \Delta PE_{surface} + \Delta KE_{surface} + \Delta(PV) + \Delta KE_{macro\ film} \quad (2)$$

and W_d is calculated by

$$W_d = \sum_{t=1}^{N_t} \sum_{s=1}^{N_s} \sum_{l=1}^{N_l} \frac{\partial U_{ls}}{\partial r_{ls}} \delta r \quad (3)$$

where ΔPE and ΔKE are the change of potential and thermal kinetic energy of the molecules in the system, respectively (molecules of different species are denoted by the subscript). Δ(PV) is the work done due to volume expansion, and $\Delta KE_{macro\ film}$ is the change in overall kinetic energy of the mean molecular motion. N_s and N_l are the number of solid and liquid molecules, respectively, and N_t is the number of molecular dynamics time steps. U_{lj} is the intermolecular potential between solid and liquid molecules, separated by a distance r_{ls}, and δr is the surface displacement during a time step. Figure 4A shows the time variation of the individual energy contributions, whereas Figure 4B shows the time evolution of ΔE_{total} and W_d. Here, the excellent agreement of ΔE_{total} with W_d validates the present model and shows that the energy transfer to the system is higher for the hydrophilic surface compared to the hydrophobic surface (for identical a and f), since W_d has direct dependence on the solid−liquid interaction strength U_{lj} (see eq 3).

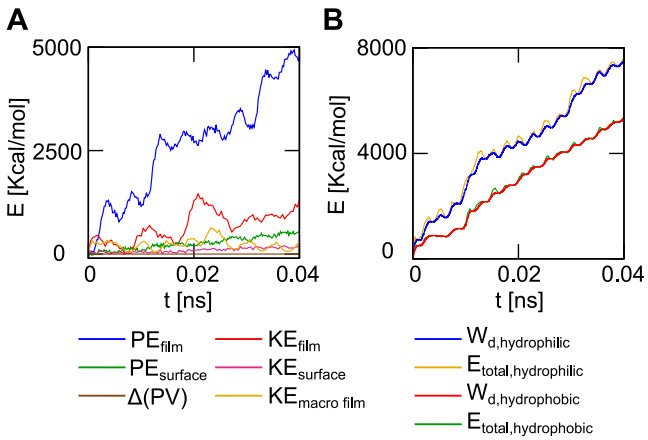

Figure 4. (A) Evolution of the contributions from individual energy components with time for a = 0.3 nm and f = 200 GHz; (B) time variation of total energy gain and work dissipated on hydrophilic and hydrophobic surfaces with a = 0.3 nm and f = 200 GHz. To reduce the computational cost, the span of the solid surface considered here is 4.7 nm (smaller compared to the span primarily used in this investigation). The independence of the phenomenon from the span of the solid surface is shown in the SI.

Figure 5 provides a comprehensive summary of our results, demonstrating the intersection between vibration parameters (a and f) and wettability (hydrophilic and hydrophobic) on one hand and mechanisms of phase transition on the other (boiling or cavitation). Here, the markers represent the surface wettability for which the initiation of a stable bubble is first observed across the range of a and f. The dominant phase-transition mechanism for the aforementioned first stable bubble

https://dx.doi.org/10.1021/acs.nanolett.0c03895
Nano Lett. 2021, 21, 1267−1273

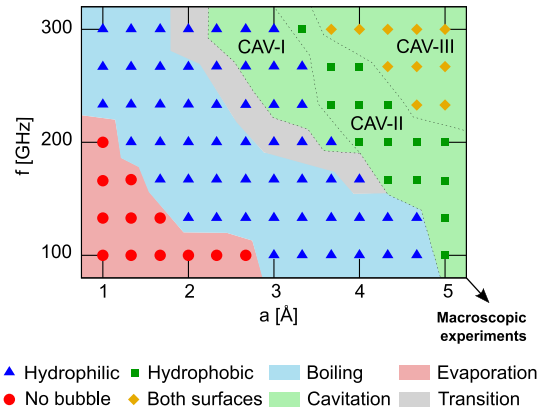

Figure 5. Regime map characterizing acoustothermal nucleation; the surface types where the initiation of a stable vapor bubble is first observed are indicated by colored markers, and the dominant phase-transition mechanism for this stable bubble is indicated by choice of background color. The black arrow indicates where current state-of-the-art macroscopic experiments (with high a ($O(0.1-1\ \mu m)$) and low f ($O(10\ kHz)$)) have been conducted.

is classified using distinct background colors. The major observations are:

(1) no stable bubble forms at low a and f (red circles) on either surface; here, the phase transition takes place only from the free liquid−vapor interface, i.e., acoustothermal evaporation (red background);

(2) in the boiling regime (blue background), formation of a stable bubble always occurs first on a hydrophilic surface (blue triangles);

(3) for moderate values of a and f, $\overline{P}_{thermal} \sim \overline{P}_{tensile}$, i.e., both cavitation and boiling are equally important, and it is difficult to distinguish between the two in our MD simulations; it is therefore classified as a transition regime (gray background); and

(4) the cavitation regime (green background) comprises three distinct zones, where initiation of nucleation takes place on hydrophilic (CAV-I), on hydrophobic (CAV-II), and simultaneously on both the surface types (CAV-III).

In the evaporation regime, the rate of work done by the vibrating solid is balanced by the energy lost from the free surface, but the energy barrier is not breached and no nucleation is observed. In the boiling regime, since the thermal motion is the dominant factor for nucleation, higher work dissipation for hydrophilic surfaces takes the liquid to a metastable state faster, producing stable vapor bubbles earlier than the comparable hydrophobic surface. The tensioning of the liquid is the dominant mode of nucleation in CAV I−III; however, the rate of total energy transfer ($W_{d,hydrophilic}$) is greater for the hydrophilic surface in CAV-I, causing faster nucleation than the hydrophobic surface. In CAV-II, a low energy barrier (i.e., $\overline{E}_{b,hydrophobic} < \overline{E}_{b,hydrophilic}$) starts gaining importance; therefore, bubbles form first on a hydrophobic surface despite a lower rate of energy input. In CAV-III, for high a and f, the energy associated with $\overline{P}_{tensile}$ becomes significantly higher than the energy barrier of either surface types and no preference for nucleation is observed.

Vibration-driven nucleation is observed in microscopic experiments with low a ($O(1\ nm)$) and high f ($O(1\ GHz)$);[46] it is also obtained in macroscopic experiments[2,3] that have been carried out in the high a ($O(0.1-1\ \mu m)$) and low f ($O(10\ kHz)$) regime. It is worth mentioning that in macroscale experiments (beyond the bottom right-hand corner of Figure 5), nucleation occurs due to high $\overline{P}_{tensile}$, i.e., cavitation. Therefore, the onset of nucleation is always quicker on hydrophobic surfaces. Both the mechanism (cavitation) and wettability (hydrophobic) are consistent with the phase map presented here (Figure 5), which provides validation of the proposed mechanisms. The phenomenon of acoustothermal nucleation is extremely rapid, so micro/nano-asperities due to surface roughness are likely not to significantly impact acoustothermal nucleation on smooth surfaces. This is similar to the case of fast nucleation in explosive boiling, where "spontaneous nucleation" due to thermal motion of the liquid molecules plays the dominant role in bubble formation.[47−49] The current study can be extended in the future to analyze the effect of surface roughness on acoustothermal nucleation.

In summary, our results address two fundamental issues that motivated this work. First, we reveal that the mechanism of acoustothermal nucleation can vary with acoustic parameters. The mechanism is dictated by how liquid molecules gain energy, which occurs via two modes, i.e., (1) by an increase of molecular kinetic energy from viscous dissipation and (2) by an increase of potential energy from film tensioning due to the surface motion. The dominance of the first mode signifies boiling, while the dominance of the second mode results in cavitation. We develop estimates for (a) an energy barrier for nucleation and (b) the work dissipated during vibration based on solid−liquid interactions, which agree very well with our simulation results. Second, despite the hydrophobic surface having a low rate of energy transfer, nucleation occurs on it because the free energy required to form a vapor nucleus is lower; this is likely when the second mode of energy gain (as mentioned above) by the liquid becomes dominant. Our study shows that changes in acoustic parameters can alter the preference of wettability for the onset of nucleation. It also reveals that vibration-induced cavitation can take place on a hydrophilic surface, i.e., it does not preferably occur always on hydrophobic surfaces, which was the previous consensus from macroscopic investigations.[2,3]

■ ASSOCIATED CONTENT

Supporting Information

The Supporting Information is available free of charge at https://pubs.acs.org/doi/10.1021/acs.nanolett.0c03895.

Details of the simulation setup, the energy barrier calculation, and the methods employed for the post-simulation measurement of relevant quantities (PDF)

■ AUTHOR INFORMATION

Corresponding Authors

Saikat Datta − *School of Engineering, University of Edinburgh, Edinburgh EH9 3FB, United Kingdom;* orcid.org/0000-0001-8962-2145; Email: saikat.mech@gmail.com

Rohit Pillai − *School of Engineering, University of Edinburgh, Edinburgh EH9 3FB, United Kingdom;* orcid.org/0000-0003-0539-7177; Email: R.Pillai@ed.ac.uk

Matthew K. Borg − *School of Engineering, University of Edinburgh, Edinburgh EH9 3FB, United Kingdom;* orcid.org/0000-0002-7740-1932; Email: Matthew.Borg@ed.ac.uk

https://dx.doi.org/10.1021/acs.nanolett.0c03895
Nano Lett. 2021, 21, 1267−1273

Khellil Sefiane − *School of Engineering, University of Edinburgh, Edinburgh EH9 3FB, United Kingdom*; Email: K.Sefiane@ed.ac.uk

Complete contact information is available at: https://pubs.acs.org/10.1021/acs.nanolett.0c03895

Notes

The authors declare no competing financial interest.

■ ACKNOWLEDGMENTS

The MD simulation results were run on ARCHER, the U.K.'s national supercomputer. This research is supported by EPSRC grants EP/N016602/1 and EP/R007438/1. The authors would like to dedicate this paper to Prof. Jason Reese, our colleague, mentor, and friend, who passed away in March 2019.

■ REFERENCES

(1) Shchukin, D. G.; Skorb, E.; Belova, V.; Moehwald, H. Ultrasonic cavitation at solid surfaces. *Adv. Mater.* **2011**, *23*, 1922−1934.
(2) Belova-Magri, V.; Brotchie, A.; Cairós, C.; Mettin, R.; Möhwald, H. Micropatterning for the control of surface cavitation: visualization through high-speed imaging. *ACS Appl. Mater. Interfaces* **2015**, *7*, 4100−4108.
(3) Belova, V.; Gorin, D. A.; Shchukin, D. G.; Möhwald, H. Controlled effect of ultrasonic cavitation on hydrophobic/hydrophilic surfaces. *ACS Appl. Mater. Interfaces* **2011**, *3*, 417−425.
(4) Zhang, L.; Belova, V.; Wang, H.; Dong, W.; Möhwald, H. Controlled cavitation at nano/microparticle surfaces. *Chem. Mater.* **2014**, *26*, 2244−2248.
(5) Maisonhaute, E.; White, P.; Compton, R. Surface acoustic cavitation understood via nanosecond electrochemistry. *J. Phys. Chem. B* **2001**, *105*, 12087−12091.
(6) Maisonhaute, E.; Brookes, B. A.; Compton, R. G. Surface acoustic cavitation understood via nanosecond electrochemistry. 2. The motion of acoustic bubbles. *J. Phys. Chem. B* **2002**, *106*, 3166−3172.
(7) Maisonhaute, E.; Prado, C.; White, P. C.; Compton, R. G. Surface acoustic cavitation understood via nanosecond electrochemistry. Part III: Shear stress in ultrasonic cleaning. *Ultrason. Sonochem.* **2002**, *9*, 297−303.
(8) Wei, Y.; Li, Y.; Zhang, N.; Shi, G.; Jin, L. Ultrasound-radiated synthesis of PAMAM-Au nanocomposites and its application on glucose biosensor. *Ultrason. Sonochem.* **2010**, *17*, 17−20.
(9) Ross, N. A.; Bartsch, R. A. High-intensity ultrasound-promoted reformatsky reactions. *J. Org. Chem.* **2003**, *68*, 360−366.
(10) Vyas, N.; Dehghani, H.; Sammons, R.; Wang, Q.; Leppinen, D.; Walmsley, A. Imaging and analysis of individual cavitation microbubbles around dental ultrasonic scalers. *Ultrasonics* **2017**, *81*, 66−72.
(11) Tachibana, K.; Tachibana, S. The use of ultrasound for drug delivery. *Echocardiography* **2001**, *18*, 323−328.
(12) Pillai, R.; Borg, M. K.; Reese, J. M. Acoustothermal atomization of water nanofilms. *Phys. Rev. Lett.* **2018**, *121*, 104502.
(13) Manor, O.; Rezk, A. R.; Friend, J. R.; Yeo, L. Y. Dynamics of liquid films exposed to high-frequency surface vibration. *Phys. Rev. E* **2015**, *91*, 053015.
(14) Kondoh, J.; Shimizu, N.; Matsui, Y.; Shiokawa, S. Liquid heating effects by SAW streaming on the piezoelectric substrate. *IEEE Transactions on Ultrasonics, Ferroelectrics, and Frequency control* **2005**, *52*, 1881−1883.
(15) Kondoh, J.; Shimizu, N.; Matsui, Y.; Sugimoto, M.; Shiokawa, S. Development of temperature-control system for liquid droplet using surface acoustic wave devices. *Sens. Actuators, A* **2009**, *149*, 292−297.
(16) Li, H.; Li, Y.; Li, Z. The heating phenomenon produced by an ultrasonic fountain. *Ultrason. Sonochem.* **1997**, *4*, 217−218.
(17) Tingaud, F.; Ferrouillat, S.; Colasson, S.; Bontemps, A.; Bulliard-Sauret, O. Experimental characterisation of the thermal behaviour of different materials submitted to ultrasound in an ultrasonic fountain. *Ultrason. Sonochem.* **2013**, *20*, 1046−1053.
(18) Tam, A. C.; Leung, W. P.; Zapka, W.; Ziemlich, W. Laser-cleaning techniques for removal of surface particulates. *J. Appl. Phys.* **1992**, *71*, 3515−3523.
(19) Morimoto, A.; Tanimura, H.; Yang, H.; Ohtsubo, S.; Kumeda, M.; Chen, X. Platinum film patterning by laser lift-off using hydrocarbon film on insulating substrates. *Appl. Phys. A: Mater. Sci. Process.* **2004**, *79*, 1015−1018.
(20) Lin, C. P.; Kelly, M. W.; Sibayan, S. A.; Latina, M. A.; Anderson, R. R. Selective cell killing by microparticle absorption of pulsed laser radiation. *IEEE J. Sel. Top. Quantum Electron.* **1999**, *5*, 963−968.
(21) Ungureanu, C.; Kroes, R.; Petersen, W.; Groothuis, T. A.; Ungureanu, F.; Janssen, H.; van Leeuwen, F. W.; Kooyman, R. P.; Manohar, S.; van Leeuwen, T. G. Light interactions with gold nanorods and cells: implications for photothermal nanotherapeutics. *Nano Lett.* **2011**, *11*, 1887−1894.
(22) Lachaine, R.; Boutopoulos, C.; Lajoie, P.-Y.; Boulais, E.; Meunier, M. Rational design of plasmonic nanoparticles for enhanced cavitation and cell perforation. *Nano Lett.* **2016**, *16*, 3187−3194.
(23) Wilson, A. M.; Mazzaferri, J.; Bergeron, E.; Patskovsky, S.; Marcoux-Valiquette, P.; Costantino, S.; Sapieha, P.; Meunier, M. In vivo laser-mediated retinal ganglion cell optoporation using KV1. 1 conjugated gold nanoparticles. *Nano Lett.* **2018**, *18*, 6981−6988.
(24) Li, M.; Lohmuller, T.; Feldmann, J. Optical injection of gold nanoparticles into living cells. *Nano Lett.* **2015**, *15*, 770−775.
(25) Neumann, O.; Neumann, A. D.; Silva, E.; Ayala-Orozco, C.; Tian, S.; Nordlander, P.; Halas, N. J. Nanoparticle-mediated, light-induced phase separations. *Nano Lett.* **2015**, *15*, 7880−7885.
(26) Huang, X.; Quinto-Su, P. A.; Gonzalez-Avila, S. R.; Wu, T.; Ohl, C.-D. Controlled manipulation and in situ mechanical measurement of single co nanowire with a laser-induced cavitation bubble. *Nano Lett.* **2010**, *10*, 3846−3851.
(27) Adleman, J. R.; Boyd, D. A.; Goodwin, D. G.; Psaltis, D. Heterogenous catalysis mediated by plasmon heating. *Nano Lett.* **2009**, *9*, 4417−4423.
(28) Levis, R. J. Laser desorption and ejection of biomolecules from the condensed phase into the gas phase. *Annu. Rev. Phys. Chem.* **1994**, *45*, 483−518.
(29) Rohsenow, W. M. *A method of correlating heat transfer data for surface boiling of liquids*, Technical Reoport No. 5; MIT Division of Industrial Cooporation: Cambridge, MA, 1951.
(30) Corty, C. Surface variables in nucleate boiling. *Chemical Engineering Progress Symposium Series* **1955**, 1−12.
(31) Bourdon, B.; Rioboo, R.; Marengo, M.; Gosselin, E.; De Coninck, J. Influence of the wettability on the boiling onset. *Langmuir* **2012**, *28*, 1618−1624.
(32) Wang, C.; Dhir, V. Effect of surface wettability on active nucleation site density during pool boiling of water on a vertical surface. *American Society of Mechanical Engineers, Heat Transfer Division* **1991**, *159*, 89−96.
(33) Takata, Y.; Hidaka, S.; Uraguchi, T. Boiling feature on a super water-repellent surface. *Heat Transfer Eng.* **2006**, *27*, 25−30.
(34) Phan, H. T.; Caney, N.; Marty, P.; Colasson, S.; Gavillet, J. Surface wettability control by nanocoating: the effects on pool boiling heat transfer and nucleation mechanism. *Int. J. Heat Mass Transfer* **2009**, *52*, 5459−5471.
(35) Nam, Y.; Wu, J.; Warrier, G.; Ju, Y. S. Experimental and numerical study of single bubble dynamics on a hydrophobic surface. *J. Heat Transfer* **2009**, *131*, 121004.
(36) Bourdon, B.; Di Marco, P.; Riobóo, R.; Marengo, M.; De Coninck, J. Enhancing the onset of pool boiling by wettability modification on nanometrically smooth surfaces. *Int. Commun. Heat Mass Transfer* **2013**, *45*, 11−15.
(37) Thomas, O. C.; Cavicchi, R. E.; Tarlov, M. J. Effect of surface wettability on fast transient microboiling behavior. *Langmuir* **2003**, *19*, 6168−6177.
(38) Balss, K. M.; Avedisian, C. T.; Cavicchi, R. E.; Tarlov, M. J. Nanosecond imaging of microboiling behavior on pulsed-heated Au films modified with hydrophilic and hydrophobic self-assembled monolayers. *Langmuir* **2005**, *21*, 10459−10467.

(39) Gong, S.; Cheng, P. Lattice Boltzmann simulations for surface wettability effects in saturated pool boiling heat transfer. *Int. J. Heat Mass Transfer* **2015**, *85*, 635−646.
(40) Yamamoto, T.; Matsumoto, M. Initial stage of nucleate boiling: molecular dynamics investigation. *J. Therm. Sci. Technol.* **2012**, *7*, 334−349.
(41) Hens, A.; Agarwal, R.; Biswas, G. Nanoscale study of boiling and evaporation in a liquid Ar film on a Pt heater using molecular dynamics simulation. *Int. J. Heat Mass Transfer* **2014**, *71*, 303−312.
(42) Zhang, H.; Li, C.; Zhao, M.; Zhu, Y.; Wang, W. Influence of interface wettability on normal and explosive boiling of ultra-thin liquid films on a heated substrate in nanoscale: a molecular dynamics study. *Micro Nano Lett.* **2017**, *12*, 843−848.
(43) Balibar, S.; Caupin, F. Metastable liquids. *J. Phys.: Condens. Matter* **2003**, *15*, S75.
(44) Carey, V.; Wemhoff, A. Thermodynamic analysis of near-wall effects on phase stability and homogeneous nucleation during rapid surface heating. *Int. J. Heat Mass Transfer* **2005**, *48*, 5431−5445.
(45) Gerweck, V.; Yadigaroglu, G. A local equation of state for a fluid in the presence of a wall and its application to rewetting. *Int. J. Heat Mass Transfer* **1992**, *35*, 1823−1832.
(46) Shilton, R. J.; Travagliati, M.; Beltram, F.; Cecchini, M. Nanoliter-droplet acoustic streaming via ultra high frequency surface acoustic waves. *Adv. Mater.* **2014**, *26*, 4941−4946.
(47) Asai, A. Bubble dynamics in boiling under high heat flux pulse heating. *J. Heat Transfer* **1991**, *113*, 973−979.
(48) Skripov, V. P. *Metastable Liquids*; translated from Russian by Kondor, R.; translation edited by Slutzkin, D.; Wiley: New York, 1974.
(49) Lin, L.; Pisano, A.; Carey, V. Thermal bubble formation on polysilicon micro resistors. *J. Heat Transfer* **1998**, *120*, 735−742.

https://dx.doi.org/10.1021/acs.nanolett.0c03895
Nano Lett. 2021, 21, 1267−1273